Neuron, Volume *97*

Supplemental Information

Neural Population Dynamics Underlying Motor Learning Transfer

Saurabh Vyas, Nir Even-Chen, Sergey D. Stavisky, Stephen I. Ryu, Paul Nuyujukian, and Krishna V. Shenoy

Neural population dynamics underlying motor learning transfer

Saurabh Vyas[1,9,*], Nir Even-Chen[2,5], Sergey D. Stavisky[2,3], Stephen I. Ryu[2,8], Paul Nuyujukian[1,2,3,5,6], and Krishna V. Shenoy[1,2,4,5,6,7]

[1]Department of Bioengineering
[2]Department of Electrical Engineering
[3]Department of Neurosurgery
[4]Department of Neurobiology
[5]Bio-X Program, Stanford University
[6]Stanford Neurosciences Institute
[7]Howard Hughes Medical Institute
Stanford University, Stanford, CA 94305, USA
[8]Palo Alto Medical Foundation, Palo Alto, CA 94301, USA
[9]Lead Contact
*Correspondence: Saurabh Vyas (smvyas@stanford.edu).

Supplemental Figures

Figure S1. *Related to Figure 1.* Uncorrelated movements during BMI use.

Figure. S2. *Related to Figure 1.* Motor adaptation transfer within and across contexts.

Figure. S3. *Related to Figures 1 and 2.* Properties of across-context adaptation transfer.

Figure S4. *Related to Figure 3.* Overt and covert movements engage a similar dynamical machine.

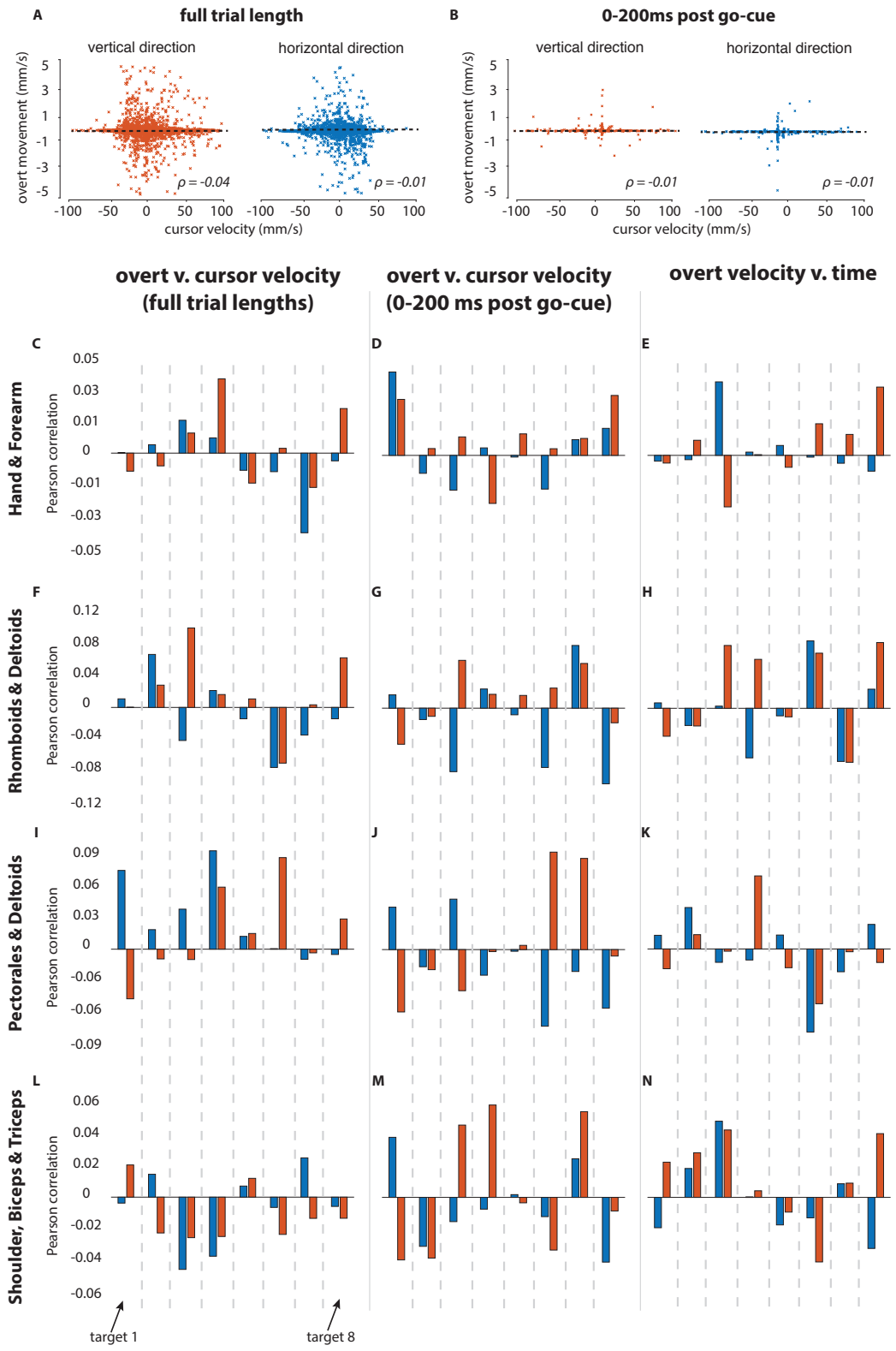

Figure S1. Related to Figure 1. Uncorrelated movements during BMI use.
A. Each point shows cursor velocity and corresponding residual overt movement velocity of a single trial during covert BMI use. Note the vastly different scale magnitudes on each axis. Overt movement velocities were experimentally measured using infrared video cameras and quantified using the Lucas-Kanade optical flow computer vision algorithm (see STAR Methods). Left and right panels correspond to

the vertical and horizontal components of the velocity, respectively. Dotted black line represents a regression fit (slopes < 1e-10), and ρ represents the Pearson correlation coefficient.
B. Same as A with the data restricted to 0-200ms immediately following the go-cue.
C. Pearson correlation coefficient as in A separated for each target for the full trial length for the hand and forearm regions. Orange and blue correspond to the vertical and horizontal components of the velocity respectively.
D. Same as C except the data is restricted to 0-200ms immediately following the go-cue as in B.
E. Pearson correlation between the overt hand and shoulder region velocity and time, separated for each target. Used to quantify movement stereotypy across trials. Colors same as C-D.
F-H. Same as C-E except for the rhomboids and deltoids regions.
I-K. Same as C-E except for the pectorales and deltoids regions.
L-N. Same as C-E except for the shoulder, biceps, and triceps regions.

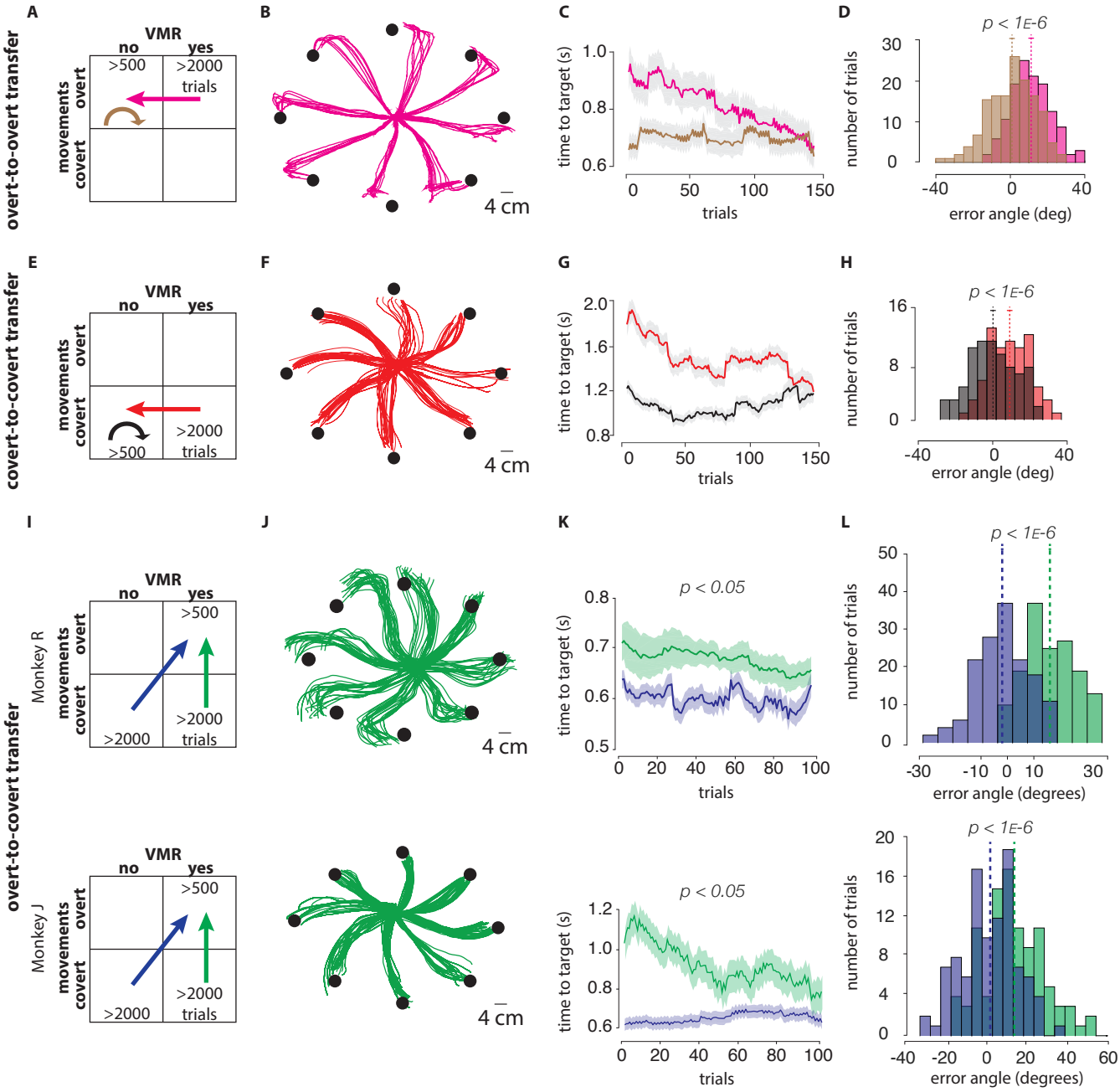

Figure. S2. Related to Figure 1. Motor adaptation transfer within and across contexts.

A. Experimental flow.

B. Raw arm-trajectories in an overt block (no VMR) following a block of overt trials (clockwise VMR applied) exhibit after-effect curvature.

C. Magenta denotes mean ± s.e.m. time to reach target in an overt block showing after-effects (overt no-VMR following overt VMR). Brown denotes control performance (overt no-VMR following overt no-VMR).

D. Error angle histograms of the arm's velocity measured at the half-way radius between the workspace center and the target. Magenta shows the experimental condition (overt trials after adapting to an overt VMR), while brown shows the control trials. *P* values were obtained from two-tailed Student's *t*-tests**.**

E-H. Same as A-D, for experiments performed entirely in the covert context.

I. Experimental flow.

J. Raw BMI-controlled cursor trajectories (no VMR applied) exhibit after-effect curvature indicating VMR transfer following adaptation to a VMR applied during preceding overt use.

K. Green trace shows the mean ± s.e.m. time to reach the target in a covert context (no-VMR) following a block of overt trials (VMR applied). Blue shows the time to reach the target in a covert context (no-VMR) following a block of overt trials (no VMR).

L. Histograms of the error angle between the arm's velocity measured at the half-way point and the straight line from workspace center to target. Green and blue correspond to the same trials as in C. Vertical dashed lines show means of distributions, and horizontal solid lines mean ± s.e.m. *P* values were obtained from two-tailed Student's *t*-tests.

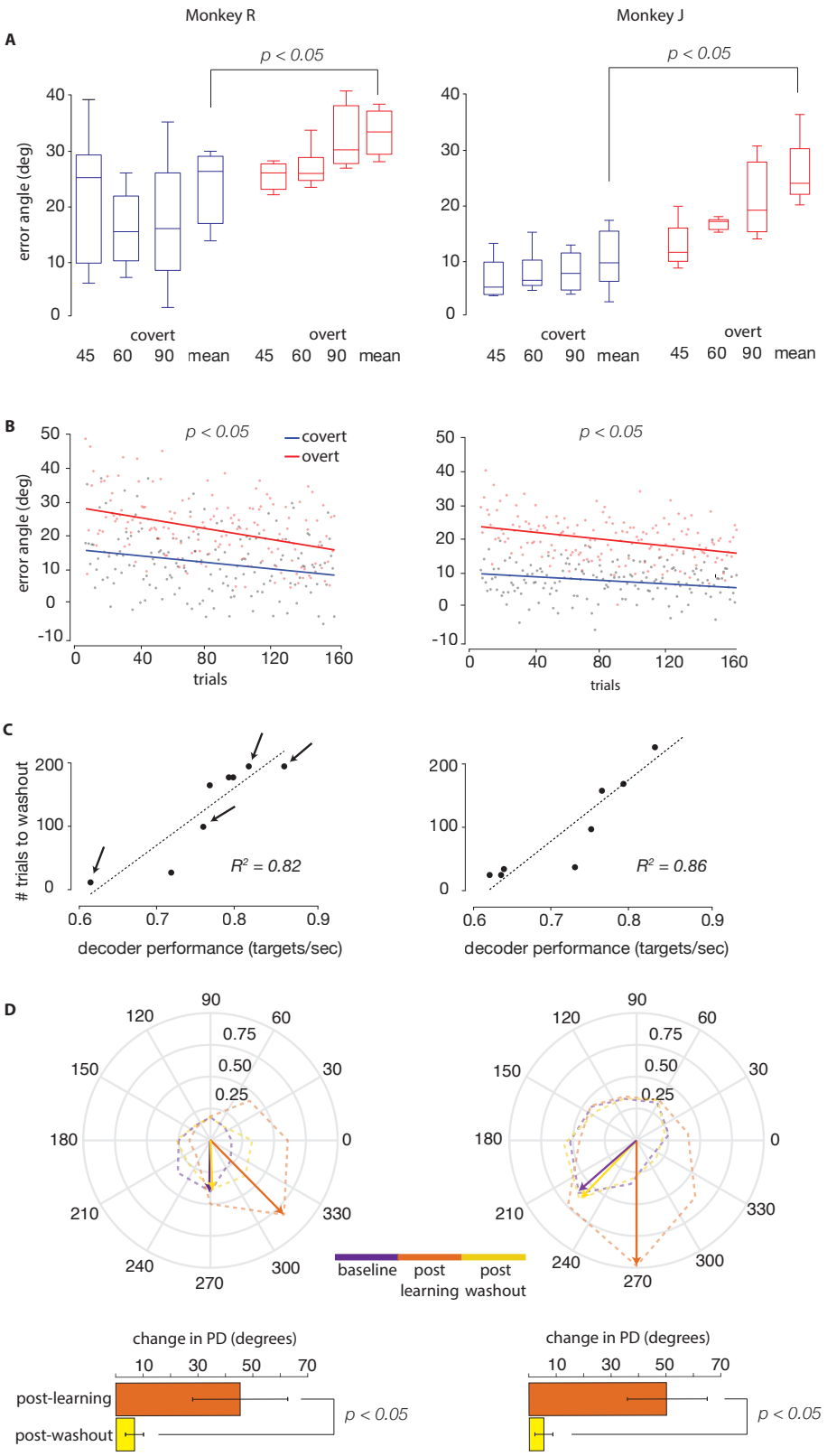

Figure. S3. Related to Figures 1 and 2. Properties of across-context adaptation transfer.
A. Error angle in the first 10 trials in an overt block (no VMR) following a block of covert (blue) or overt (red) block (VMR applied) as measured in Fig. 1. This is also shown separately for each of the three VMR

angles (45˚, 60˚, and 90˚). After-effect error, indicative of across-context adaptation transfer, was smaller than within-context effect. *P* values were obtained using the Wilcoxon rank-sum test.

B. Error angle as a function of trial number for the same conditions (red and blue) as A.

C. The *x*-axis denotes performance of the BMI decoder after adapting to a VMR (45˚, 60˚, and 90˚). The *y*-axis shows the number of overt arm-reaching trials needed to wash out VMR adaptation transfer (i.e., trials needed to reach 85% of the control performance) following the preceding block of covert trials with VMR. Higher decoder performance after adapting to VMRs is significantly correlated with higher washout magnitude ($p < 0.05$). Black arrows for Monkey R correspond to sessions where ReFIT was used. For Monkey J ReFIT was never used.

D. (Top) Example tuning curves (from one representative neuron) for the baseline (purple), post-learning (orange; final 50 learning trials), and post-washout (yellow; last 50 trials). During learning the preferred direction (PD), shown as solid arrows, rotates to presumably align with the VMR, and during washout the PD rotates back to baseline. (Bottom) Population wide statistics (for the top 50 most tuned electrodes on each array) for the change in PD (relative to baseline) for post-learning and post-washout epochs. *P* values were obtained using the Wilcoxon rank-sum test.

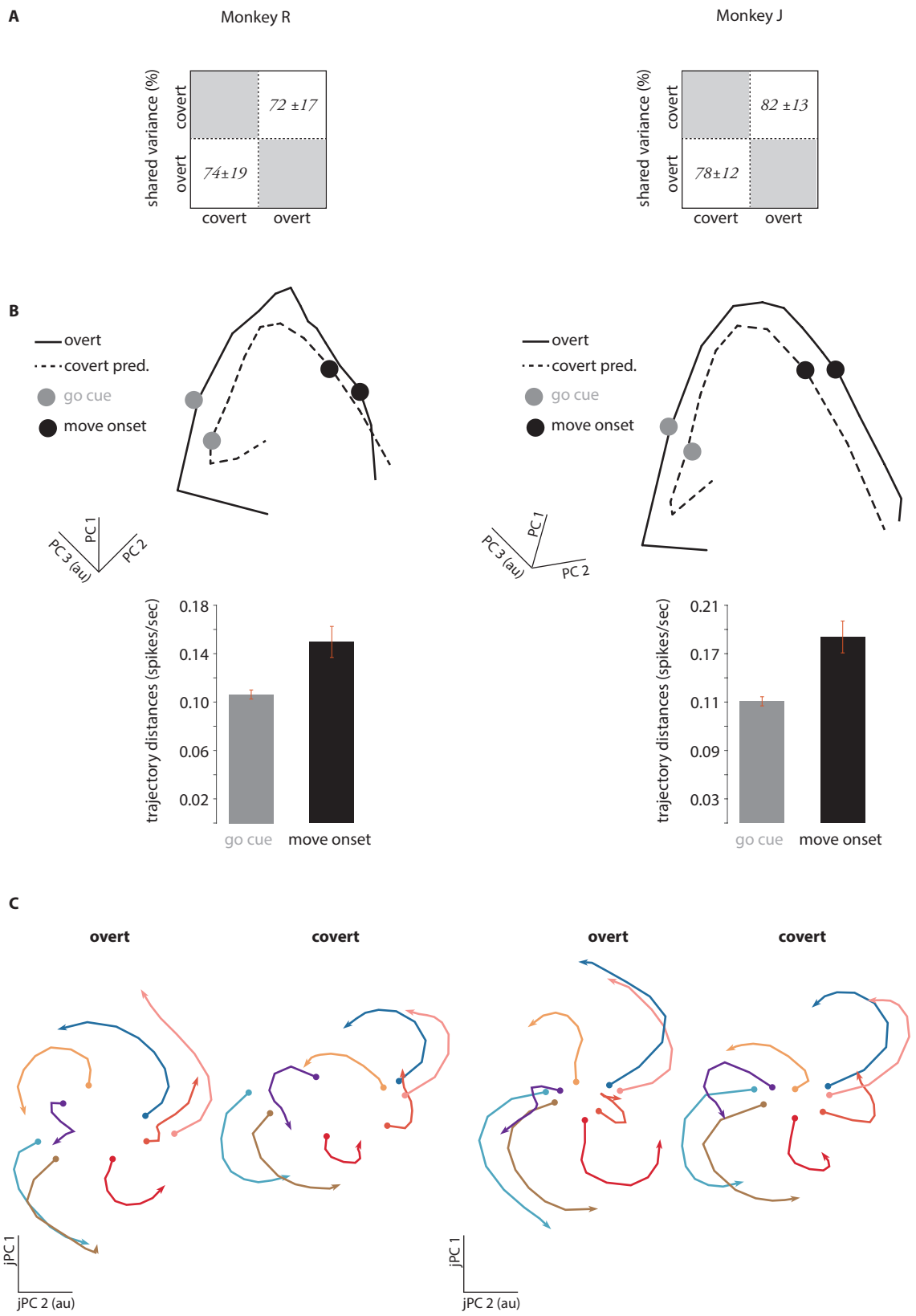

Figure S4. Related to Figure 3. Overt and covert movements engage a similar dynamical machine. A. Percentage of shared variance between the overt and covert context neural data during the movement epochs. Data from each context is projected into the other context before the calculations are done. The subspaces were comprised of PCs, which collectively captured over 90% of the total neural variance.

B. (Top) Solid lines show example neural trajectories in a three-dimensional state-space for overt arm reaches. Dotted lines show a linear dynamical system (LDS) fit of covert data, initialized using the initial condition (i.e., preparatory state) from the *overt* context and the resulting dynamics are projected into the overt movement state-space. Gray and black circles show the time of go-cue and movement onset, respectively. These plots support the interpretation that a LDS fit on covert data can well predict overt dynamics when seeded with the overt initial condition. (Bottom) Differences between the full-dimensional trajectories at the go-cue and movement onset conditions. Error bars show the 5th and 95th percentile of the distribution.

C. Projections of the population response onto the first two jPCs for 200ms of neural data aligned to the go-cue. Each trace corresponds to a different reach condition; colors matched to Figure 3. These plots support the interpretation that the oscillatory component in motor cortical population responses observed during overt reaching is also observed during covert movements.